Macromolecules **2002,** *35,* 135−140

NMR Imaging Study of Stress-Induced Material Response in Rubber Modified Polyamide 6

P. Adriaensens, L. Storme, R. Carleer, J. D'Haen, and J. Gelan*

Limburg University, Institute for Materialresearch (IMO), Department SBG, Universitaire Campus, Building D, B-3590 Diepenbeek, Belgium

V. M. Litvinov,[†] R. Marissen,[†,‡] and J. Crevecoeur[†]

DSM Research, P.O. Box 18, 6160 MD Geleen, The Netherlands, and Delft University of Technology, Faculty of Mechanical Engineering, Mekelweg 2 2628 CD Delft, The Netherlands

Received July 25, 2001

ABSTRACT: The fracture behavior of two different types of extruded polyamide 6 (PA6)/maleic anhydride grafted ethylene−propylene (EPM-*g*-MA) blends is examined by magnetic resonance imaging (MRI). TEM micrographs demonstrate a clear difference in morphology: where one blend type contains pure rubber particles dispersed in the PA6 matrix, the other type contains PA6 occlusions within the rubber particles and is significantly more tough. MRI experiments on notched specimens of both blend types under critical load reveal a gradual increase of rubber cavitation toward the crack tip which can be quantified on the basis of the localized proton spin density. A clear relation is observed between the toughness and the dimensions of the plastic zone: the toughest blend has a significant more extended plastic zone ahead of the crack tip. The enhanced toughness of the blends with occlusions can be attributed to a more pronounced delocalization of energy, which is suggested to result from a different deformation mechanism in which the load bearing capacity of the rubbery chains plays an important role.

Introduction

Polyamides (PA) are well-known as strong engineering polymers. They exhibit high resistance to crack initiation, which imparts high toughness to unnotched material. However, their low resistance to crack propagation leads to embrittlement in the presence of a notch. Upon modification with rubbers, the resistance to crack propagation increases, leading to tough materials. Previous research on rubber toughened polyamides mainly focused on the influence of the particle size, the interparticle distance, the cavitation behavior, the rubber concentration, and the rubber−matrix interfaces on the toughening effect.[1−7] The role of rubber particles in the toughening of semicrystalline polymers is now understood rather well.[8−14] Rubber particles enhance plastic deformation and promote cavitation. Both mechanisms result in enhanced toughness by the formation of a plastic zone in front of the crack tip, which blunts the sharp crack. Consequently, cracking and crazing are suppressed. During this process, the cavitated rubber particles will change substantially in shape and in volume.[14,15] Ideally, the plastic deformation is activated in the entire matrix, resulting in massive energy dissipation and hence improved fracture toughness. For rubber toughened polyamide 6.6, Bucknall et al. demonstrated the acceleration of local plastic deformation of the matrix by cavitation.[15,16]

The spin-warp NMR imaging technique, which detects only the soft phase in polymer materials, has been demonstrated to be a useful tool to study the resistance to crack growth in polymers.[17] Although the spatial resolution of MRI, being about 50 μm or less,[18−20] is rather limited as compared to TEM and SEM, the method provides complementary information because of the large variety of molecular dependent contrast parameters, like the spin density (M_0) and the relaxation times $T_{1\mathrm{H}}$ (spin−lattice relaxation time), $T_{1\rho\mathrm{H}}$ (spin−lattice relaxation time in the rotating frame), and $T_{2\mathrm{H}}$ (spin−spin relaxation time).[21−23] These parameters can be related to the spatially dependent amount of soft phase and molecular mobility of polymer chains. Quantitative images of the spin density and relaxation times can be of particular interest for the understanding of the mechanism of a growing crack.

In the present study the difference in fracture behavior of two different types of polyamide 6 (PA6) specimen are examined in which maleic anhydride grafted ethylene−propylene rubber (EPM-*g*-MA) is dispersed in the PA6 matrix. One type of blends contains PA6 occlusions in the rubbery phase in different proportions; the other type is free of occlusions. For the blend free of occlusions, the reaction of the amino end groups of PA6 with the grafted maleic anhydride functionality of the EPM rubber only occurs at the interface of the rubber particle and the PA6 matrix, giving rise to the formation of a graft copolymer and resulting in a compatibilizing effect. For the blends with PA6 occlusions in the rubbery phase this reaction additionally takes place at the rubber−PA6 interface of the occluded PA6 particles.[24,25]

Experimental Section

Materials. Two types of PA6-*blend*-(EPM-*g*-MA) blends were investigated. One type of blends consists of pure EPM-*g*-MA rubber dispersed in the PA6 matrix and is represented by a sample containing 20 wt % dispersed phase and which is designated as the standard blend (Bl-st). In the other type of blends, PA6 occlusions are introduced in the dispersed rubbery phase (Bl-oc). Bl-oc1 contains 20 wt % dispersed phase (14 wt % EPM-*g*-MA) while a larger amount of 28 wt % (20 wt % EPM-*g*-MA) is introduced in Bl-oc2. An overview is presented in Table 1.

[†] DSM Research.
[‡] Delft University of Technology.
* To whom correspondence should be addressed.

10.1021/ma0113273 CCC: $22.00

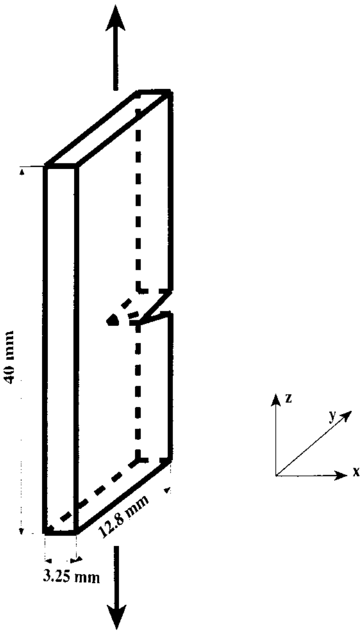

Figure 1. Sample shape showing the 4 mm notch and its position in the magnet with respect to the B_0 field (z-direction). Loading is applied parallel to the z-direction.

Table 1. Composition of the PA6/EPM-*g*-MA Blends

	EPM-*g*-MA (wt %)	occluded PA6 (wt %)	dispersed phase (wt %)
Bl-st	20		20
Bl-oc1	14	6	20
Bl-oc2	20	8.6	28.6

The compounds have been prepared on a corotating Werner & Pfleiderer twin screw extruder (ZSK 30). The screws were equipped with two kneading sections in order to properly melt and disperse the components. The temperature was set at 260 °C, and the screw speed amounted to 250 rpm. The throughput was 12 kg/h, resulting in a torque of 80%. All components were fed at the throat of the extruder. The melt temperature at the die was approximately 280 °C. Both compounds were degassed during extrusion.

MRI measurements were accomplished on rectangular plates with a dimension of 40 × 12.8 × 3.25 mm. The plates were sharply notched (4 mm in depth) perpendicular to the strain direction (z) to obtain the condition of a growing crack (Figure 1). Loading of the notched plates was accomplished in a “home-developed” stretching device[17] that fits in the MRI probehead.

Imaging. MRI images were acquired at 9.4 T in an Inova 400 Varian vertical bore spectrometer. A 16 mm coil insert was used in the microimaging probe. All images have an inplane pixel resolution of about 120 × 120 μm in a field of view of 16 × 20 mm. A spin-warp pulse sequence with a repetition delay (TR) of 3 s and an echo time (TE) of 1.1 ms was used.[19] Image slices of 2.5 mm in thickness were selected in the middle of the specimen by tuning the offset frequency in the slice direction. Typical gradient strengths used were 27, 8, and 18 G/cm for phase, read, and slice direction, respectively.

The local spin density (M_0) and spin−spin relaxation time (T_{2H}) were determined by analyzing the local echo amplitude as a function of TE (15 values between 1.10 and 2 ms) with a fixed TR of 2 s, using the following relation:

$$\ln M(\mathrm{TE}) = \ln M_0 - \mathrm{TE}/T_{2H} \tag{1}$$

The spatial dependence of the spin−lattice relaxation time (T_{1H}) and M_0 were determined from a series of images taken as a function of TR (10 values between 0.25 and 3.5 s) with a fixed TE of 1.10 ms, according to the following relation:[26]

$$M(\mathrm{TR}) = M_0(1 - \mathrm{e}^{-\mathrm{TR}/T_{1H}})\mathrm{e}^{-\mathrm{TE}/T_{2H}} \tag{2}$$

The localized values of M_0, T_{2H}, and T_{1H} are compared to their reference values, which are represented by the average of 10 unaffected locations. All images visualize selectively the rubber phase since the transverse magnetization of the glassy PA6 matrix, which decays to zero within 100 μs, is filtered by the rather long spin echo time (TE).

The determination of the T_{2H} relaxation time as a function of the angle between the strain direction and the static magnetic field B_0 was accomplished on a small rectangular specimen, cut in the proximity of the crack tip. The specimen was rotated over 90° in several steps, and the intensities of 1D projections were analyzed as a function of TE (15 values between 1.1 and 2 ms).

Transmission Electron Microscopy. The morphology of undeformed specimens was studied by means of transmission electron microscopy. Samples were trimmed and subsequently stained with a 1:1 OsO_4/formaline mixture. Sections of 70 nm were cut at −110 °C and studied in a JEOL 2000FX transmission electron microscope.

Scanning Electron Microscopy. Specimens for scanning electron microscopy were prepared from loaded samples that were used for the MRI experiments. To ensure no preparation artifacts, only a carbon coating on the sample surface (without polishing up) is applied before studying the morphology near to the crack tip. The study was performed with a Philips XL30FEG scanning electron microscope.

Impact Test. The notched charpy impact tests were executed according to the ISO 179 standard at 23 and −30 °C.

Tensile Test. The tensile tests were executed according to the ISO 527/1A at 50 mm/min and room temperature.

Results and Discussion

In this paper, attention is focused on the difference in toughness behavior of two types of extruded PA6-EPM-*g*-MA blends (Table 1), which were prepared by using a different compounding process. Clear differences are observed in the morphology of the specimens as demonstrated by TEM micrography (Figure 2). Whereas in the standard blend (Bl-st) homogeneous rubber particles are dispersed into the PA6 matrix (Figure 2a), the rubber particles of the occluded type of blends (Bl-oc1 and Bl-oc2) show a “salami”-type structure caused by the PA6 occlusions introduced in the dispersed phase (Figure 2b,c). Having the same volume fraction of dispersed phase, the Bl-oc1 blend is more tough as compared to Bl-st (Table 2) despite its lower rubber content and higher E modulus (Table 3). According to Oshinski et al., nonoccluded blends having a 20 wt % dispersed rubbery phase content only reach their optimal impact strength (73 kJ/m^2) if a narrow particle size distribution of around 200−300 nm is present.[4] Both the Bl-st and Bl-oc1 blends are not situated in this optimal region due to the presence of a rather broad particle size distribution (Figure 2). This means that the impact strength probably can be further improved by increasing the volume fraction of the dispersed phase. The Bl-oc2 blend, having a higher volume fraction of the dispersed phase, yields the highest toughness and lowest E modulus. The goal of this study is to explain the improved toughness of the blends containing PA6 occlusions in the dispersed rubbery phase from a molecular point of view.

Scanning electron micrographs (SEM) of blend plates that were strained to yield stress clearly show cavitation of the rubber particles in the deformation zone ahead of the starter crack (Figure 3). As is extensively de-

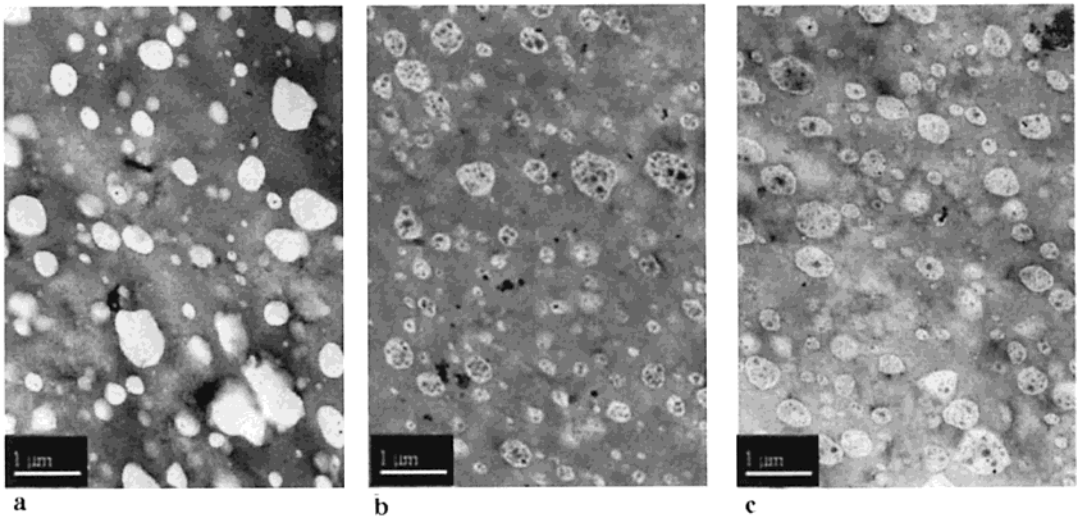

Figure 2. Transmission electron micrographs of the Bl-st (a), the Bl-oc1 (b), and the Bl-oc2 (c) blends.

Table 2. Results of the Notched Charpy Impact Test As Determined According to the ISO 179 Standard

	I (kJ/m^2)		
temp (°C)	Bl-st	Bl-oc1	Bl-oc2
23	39.9 ± 0.8	51.6 ± 0.3	78.0 ± 1.4
−30	16.1 ± 1.1	N.D.	24.1 ± 0.7

Table 3. Tensile Properties As Determined According to the ISO 527 Standard at a Rate of 50 mm/min

mechanical properties	Bl-st	Bl-oc1	Bl-oc2
E modulus (N/mm^2)	2052 ± 52	2266 ± 37	1820 ± 36
yield stress (N/mm^2)	50.95 ± 0.22	58.08 ± 0.24	45.76 ± 0.17
yield strain (%)	3.96 ± 0.10	3.94 ± 0.06	4.02 ± 0.02
stress at break (N/mm^2)	41.23 ± 1.24	41.75 ± 0.60	39.85 ± 1.05
strain at break (%)	32.10 ± 5.24	36.96 ± 11.92	29.33 ± 8.05

scribed in the literature, cavitation is an important energy dissipating deformation mechanism in rubber toughened thermoplastic materials.[27,28] Upon loading, the rubber particles become elongated and enlarged as can be judged from the shape and dimension of the cavities. The elongation of the rubber particles, along the direction of local deformation of the PA6 matrix,[29] results in void growth due to high stress near the crack tip. Cavity walls are lined with a layer of rubber as demonstrated by Pearson et al. by means of backscattered electron imaging.[12] It is clear that the macroscopically observed stress whitening results mainly from simple void growth rather than from multiple crazing.

Parts a and b of Figure 4 present the MRI images of the Bl-st and Bl-oc2 blends under critical load, respectively. The stress-induced material response ahead of the crack tip can be differentiated as a hypointense deformation zone. An appreciable larger deformation zone is observed for the Bl-oc2 blend as compared to the Bl-st blend. This improved dissipation of stress energy confirms the big gain in toughness for the occluded blend. The stress-induced material response is quite irreversible as can be judged from the images obtained after unloading (Figure 4c,d). Images of notched plates that were drawn to yield stress on a commercial straining instrument show identical dimensions of stress-induced material response and confirm that critical load is retained during the MRI experiment.

Since image intensity can be a rather complex function of the local concentration of protons of the rubbery material (M_0) and the T_{1H} and T_{2H} relaxation times, the spatial dependence of these MRI contrast parameters was investigated in order to determine whether the hypointensity of the deformation zone is caused by cavitation and/or strain-induced molecular chain elongation of the rubbery chains.[30] Please keep in mind that these images only visualize the rubbery phase since the rather long echo time (1.1 ms) acts as a highly selective T_{2H} relaxation time filter, excluding the fast T_{2H} decaying PA6 proton magnetization. Therefore, the spatial-dependent proton spin density (M_0) is directly related to the local amount of rubber. Concerning the relaxation of elastomers, the spin−spin relaxation time T_{2H} provides information about the slow, large-scale chain mobility while the spin−lattice relaxation time T_{1H} is sensitive toward the fast, local mobility. (Spectroscopic solid-echo proton wide-line T_{1H} measurements demonstrate that spin diffusion of proton magnetization[31] is not taking place efficiently between the PA6 matrix and the dispersed rubbery phase in these blend materials.)

Table 4 shows the localized values of the MRI parameters obtained for the Bl-st blend under load and after unloading (Figure 5; locations 1−6). The values determined for the Bl-oc2 blend, having a more extended damage zone (Figure 5; locations 1−9), are presented in Table 5. The average reference values, derived from several undeformed locations, are given for comparison.

For both the Bl-st and Bl-oc2 blends, a significant decrease of the proton spin density (locations 1−6) is observed in the deformation zone as compared to the undeformed locations. This decrease in spin density, which becomes more pronounced toward the notch tip, provides a measure of the degree of cavitation of the rubbery particles. In the plastic zone, a gradual increase of rubber cavitation takes place toward the tip of the starter crack. Although close to the crack tip (locations 1−6), the amount of cavitation is quite similar for both blends; the volume affected by cavitation is more extended for Bl-oc2 (locations 7−9). Unloading of the samples results in a slight recovery of the spin density but almost only for the locations 3, 6, and 9, which are situated at the border of the damage zone.

Concerning the T_{1H} relaxation, no significant differences are detected in the stress-whitened zone as compared to the unaffected locations. This means that the fast, local mobility of the noncavitated rubber

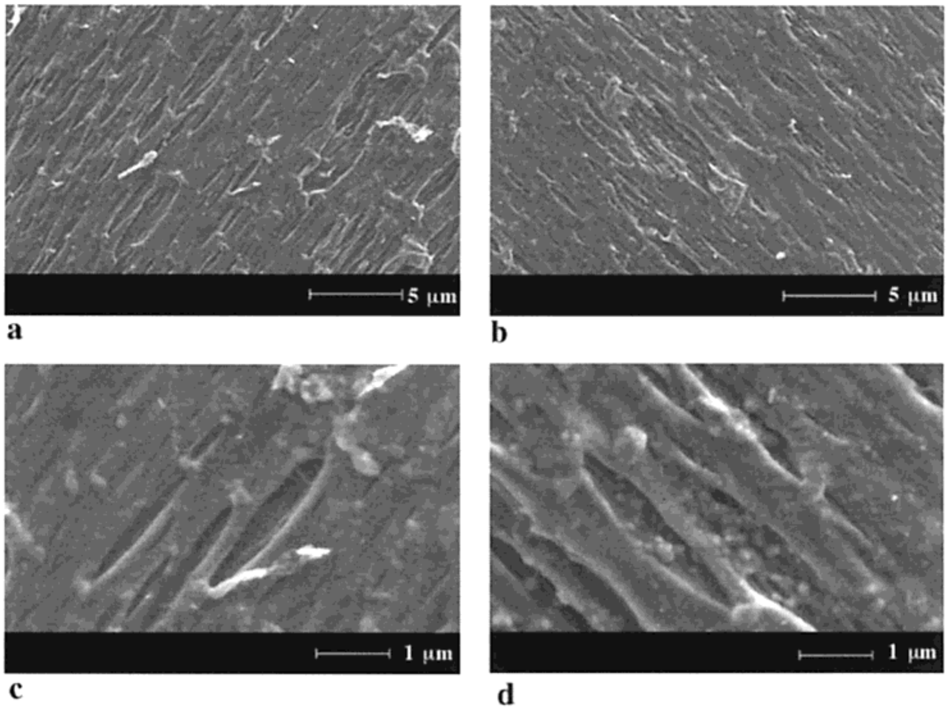

Figure 3. Scanning electron micrographs of the deformation zone ahead of the crack tip of the Bl-st blend (a, c) and of the Bl-oc2 blend (b, d) both strained to yield stress.

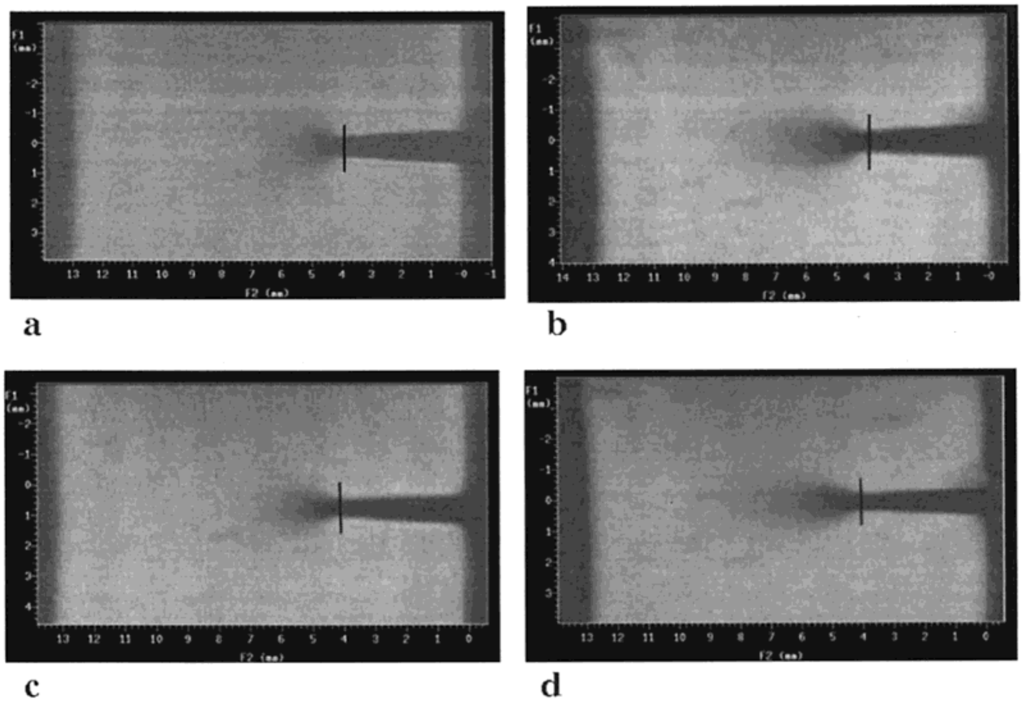

Figure 4. (a, b) MRI images of the Bl-st and Bl-oc2 blends under critical load, respectively. (c, d) Images of the Bl-st and Bl-oc2 blends after unloading, respectively (TE = 1.10 ms, TR = 3 s). A vertical bar indicates the depth of the original notch (4 mm).

chains, which probably is dominated by fast methyl group rotation, is hardly affected by the applied stress.

As far as T_{2H} relaxation is concerned, no significant changes are observed in the deformation zone of the Bl-st blend as compared to the average reference value. It means that no stress-induced chain elongation takes place in this blend. For Bl-oc2, on the other hand, the T_{2H} decay of the proton spins in the plastic zone is significantly faster as compared to this of the unaffected locations and this as well under load as after unloading. This faster relaxation of rubbery protons can be assigned to a drop in the long-range mobility of the rubbery chains. In contrast to Bl-st, for which the molecular chain mobility is mainly determined by entanglements, the occlusions in Bl-oc2 not only result in a larger amount of interphase but also introduce topological constraints that can result in strain amplification similar to that observed in filled rubbers.[32] While the hypointensity observed in the deformation zone for Bl-st can fully be assigned to the reduction in rubber spin density (cavitation), for Bl-oc2 both cavitation and stress-induced chain elongation contribute to

Table 4. Spatial Dependence of the Spin Density (M_0) and T_{2H} and T_{1H} Relaxation Times under Critical Load and after Unloading for the Bl-st Blend[a,b]

spatial locations	loaded		unloaded		loaded		unloaded	
	T_{2H} (ms)	M_0	T_{2H} (ms)	M_0	T_{1H} (s)	M_0	T_{1H} (s)	M_0
1	0.93	23	0.91	25	0.64	21	0.64	26
2	0.98	21	0.98	19	0.61	18	0.59	25
3	0.89	36	0.92	52	0.66	35	0.62	52
4	0.91	35	0.89	35	0.63	31	0.63	37
5	0.91	31	0.90	33	0.54	28	0.65	31
6	0.88	35	0.94	51	0.66	35	0.64	53
reference	0.93	100	0.96	100	0.63	100	0.68	100

[a] The spatial locations are indicated in Figure 5. [b] The averaged 95% confidence limit for T_{1H}, T_{2H}, and M_0 is about 5%, 8%, and 8%, respectively.

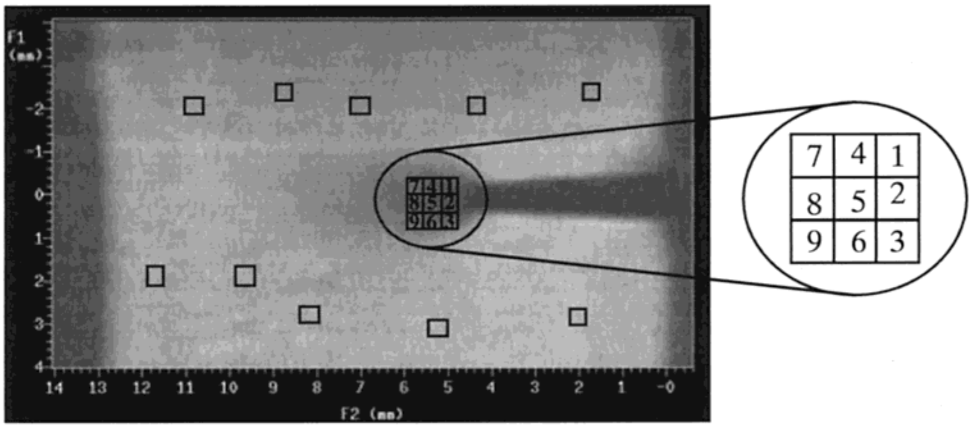

Figure 5. MRI image of the Bl-oc2 blend under critical load. The numbered locations correspond to the spatial locations for which the quantitative spin density (M_0), and the T_{1H} and T_{2H} relaxation times were determined. The unmarked squares represent the locations which were used to obtain the T_{1H} and T_{2H} reference values (see Tables 4 and 5).

Table 5. Spatial Dependence of the Spin Density (M_0) and T_{2H} and T_{1H} Relaxation Times under Critical Load and after Unloading for the Bl-oc2 Blend[a,b]

spatial location	loaded		unloaded		loaded		unloaded	
	T_{2H} (ms)	M_0	T_{2H} (ms)	M_0	T_{1H} (s)	M_0	T_{1H} (s)	M_0
1	0.69	27	0.73	34	0.68	27	0.62	27
2	0.74	18	0.78	17	0.67	20	0.61	20
3	0.70	31	0.72	45	0.62	33	0.59	44
4	0.67	36	0.67	45	0.67	38	0.65	41
5	0.61	41	0.62	39	0.62	40	0.60	39
6	0.65	40	0.63	50	0.63	44	0.61	54
7	0.71	48	0.74	46	0.68	50	0.65	51
8	0.67	51	0.70	48	0.66	51	0.64	52
9	0.65	59	0.62	70	0.65	64	0.61	74
reference	0.81	100	0.83	100	0.66	100	0.61	100

[a] The spatial locations are indicated in Figure 5. [a] The averaged 95% confidence limit for T_{1H}, T_{2H}, and M_0 is about 5%, 8%, and 8%, respectively.

the hypointensity. However, while the degree of cavitation drops toward the borders of the deformation zone, the degree of stress-induced chain elongation seems to be spatially independent in the damage zone. It is suggested that the physical/topological constraints, introduced by the occlusions, result in a different deformation mechanism in which the load bearing capacity of the rubbery chains has an important contribution. A deformation mechanism in which the rubber particles not only promote cavitation but also carry a load bearing capacity can explain the improved toughness of the occluded blends. Although Bl-oc1 has a similar volume fraction of dispersed phase (but less rubber) as compared to Bl-st, an improvement in impact strength of about 12 kJ/m^2 is reached at a similar particle size distribution. Although the increased volume fraction of dispersed phase in Bl-oc2 will certainly contribute to the improved toughness of this blend,[33] a high impact strength of 78 kJ/m^2 is obtained despite of the broad particle size distribution.

To examine whether some overall preferential orientation direction of the rubbery chains is present in the occluded blends, the T_{2H} decay value was evaluated as a function of the angle between the strain direction and the static magnetic field B_0. No angular dependency of the T_{2H} relaxation time however was observed, indicating that no overall preferential orientation of the rubbery chains takes place within the deformation volume (2 × 2 × 4 mm) ahead of the crack tip.

Conclusions

This MRI study indicates a difference in the deformation mechanism for extruded PA6-EPM-*g*-MA blends with and without PA6 occlusions in the rubbery phase. Stress-induced elongation of the rubbery chains, caused by physical and topological constraints, results in an improved impact strength for the occluded blends that originates from the load bearing capacity of the rubbery chains as is demonstrated by the localized T_{2H} decay times. The toughness of the occluded type blends is not solely provided by simple rubber cavitation, which can be quantified by means of the localized proton spin density, but is significantly enhanced by a more pronounced delocalization of the local strain as a result of favorable conditions for stress-induced chain elongation of the rubbery chains.

Acknowledgment. The authors are thankful to the European Community (“Europees Fonds voor Regionale Ontwikkeling”) and the Limburgfonds (GOM Limburg) for the financial support, to J. Kaelen for the technical support in constructing the stretching device, and to Ir. L. Naelaerts for the tensile stress measurements.

References and Notes

(1) Hobbs, S. Y.; Bopp, R. C.; Watkins, V. H. *Polym. Eng. Sci.* **1983**, *23*, 380.
(2) Wu, S. *J. Appl. Polym. Sci.* **1988**, *35*, 549.
(3) Borggreve, R. J. M.; Gaymans, R. J. *Polymer* **1989**, *30*, 63.
(4) Oshinski, A. J.; Keskkula, H.; Paul, D. R. *Polymer* **1992**, *33*, 267.
(5) Dijkstra, K.; Laak, J.; Gaymans, R. J. *Polymer* **1994**, *35*, 315.
(6) Muratoglu, O. K.; Argon, A. S.; Cohen, R. E.; Weinberg, M. *Polymer* **1995**, *36*, 4771.
(7) Kudva, R. A.; Keskkula, H.; Paul, D. R. *Polymer* **2000**, *41*, 335.
(8) Bucknall, C. B.; Rizzieri, R.; Moore, D. R. *Polymer-Letchwork* **2000**, *41*, 4149.
(9) Bucknall, C. B.; Ayre, D. S.; Dijkstra, D. J. *Polymer-Letchwork* **2000**, *41*, 5937.
(10) Sugimoto, M.; Ishikawa, M.; Hatada, K. *Polymer* **1995**, *36*, 3675.
(11) Yee, A. F.; Pearson, R. A. *J. Mater. Sci.* **1986**, *21*, 2462.
(12) Pearson, R. A.; Yee, A. F. *J. Mater. Sci.* **1986**, *21*, 2475.
(13) Steenbrink, A. C.; Litvinov, V. M.; Gaymans, R. J. *Polymer* **1998**, *39*, 4817.
(14) Pijnenburg, K. G. W.; Steenbrink, A. C.; Van der Giessen, E. *Polymer* **1999**, *40*, 5761.
(15) Bucknall, C. B.; Heather, P. S.; Lazzeri, A. *J. Mater. Sci.* **1989**, *16*, 2255.
(16) Bucknall, C. B.; Lazzeiri, A. *J. Mater. Sci.* **2000**, *35*, 427.
(17) Adriaensens, P.; Storme, L.; Carleer, R.; Vanderzande, D.; Gelan, J.; Litvinov, V. M.; Marissen, R. *Macromolecules* **2000**, *33*, 4836.
(18) Blümich, B., Kuhn, W., Eds. *Magnetic Resonance Microscopy: Methods and Applications in Materials Science, Agriculture and Biomedicine;* VCH Publishers: New York, 1992.
(19) Callaghan, P. T. *Principles of Nuclear Magnetic Resonance Microscopy*; Clarendar Press: Oxford, 1991.
(20) Kuhn, W. *Angew. Chem., Int. Ed. Engl.* **1990**, *29*, 1.
(21) Blümler, P.; Blümich, B. *Acta Polym.* **1993**, *44*, 125.
(22) Adriaensens, P.; Pollaris, A.; Vanderzande, D.; Gelan, J.; White, J. L.; Dias, A. J.; Kelchtermans, M. *Macromolecules* **1999**, *32*, 4692.
(23) Ercken, M.; Adriaensens, P.; Vanderzande, D.; Gelan, J. *Macromolecules* **1995**, *28*, 8541.
(24) Thomas, S.; Groeninckx, G. *Polymer* **1999**, *40*, 5799.
(25) Borggreve, R. J. M.; Gaymans, R. J.; Schuijer, J. *Polymer* **1989**, *30*, 71.
(26) Liu, J.; Nieminen, A. O. K.; Koenig, J. L. *J. Magn. Reson.* **1989**, *85*, 95.
(27) Ishikawa, M.; Chiba, I. *Polymer* **1982**, *23*, 291.
(28) Ishikawa, M. *Polymer* **1995**, *36*, 2203.
(29) Giaconi, G. F.; Castellani, L.; Maestrini, C.; Riccò, T. *Polymer* **1998**, *39*, 6315.
(30) Schneider, M.; Demco, D. E.; Blümich, B. *Macromolecules* **2001**, *34*, 4019.
(31) Komoroscki, R. A. *High Resolution NMR Spectroscopy of Synthetic Polymers in Bulk*; VCH: New York, 1986.
(32) Litvinov, V. M.; Steeman, P. A. M. *Macromolecules* **1999**, *32*, 8476.
(33) Bucknall, C. B. *Toughened Plastics*; Applied Science Publishers Ltd.: London, 1977.

MA0113273